Journal of Biomedical Optics

BiomedicalOptics.SPIEDigitalLibrary.org

Virtual unfolding of light sheet fluorescence microscopy dataset for quantitative analysis of the mouse intestine

Alessia Candeo
Ilenia Sana
Eleonora Ferrari
Luigi Maiuri
Cosimo D'Andrea
Gianluca Valentini
Andrea Bassi

SPIE.

Alessia Candeo, Ilenia Sana, Eleonora Ferrari, Luigi Maiuri, Cosimo D'Andrea, Gianluca Valentini, Andrea Bassi, "Virtual unfolding of light sheet fluorescence microscopy dataset for quantitative analysis of the mouse intestine," *J. Biomed. Opt.* **21**(5), 056001 (2016), doi: 10.1117/1.JBO.21.5.056001.

Virtual unfolding of light sheet fluorescence microscopy dataset for quantitative analysis of the mouse intestine

Alessia Candeo,[a] Ilenia Sana,[b] Eleonora Ferrari,[b] Luigi Maiuri,[b,c] Cosimo D'Andrea,[a] Gianluca Valentini,[a] and Andrea Bassi[a,*]
[a]Politecnico di Milano, Dipartimento di Fisica, piazza Leonardo da Vinci 32, 20133 Milano, Italy
[b]European Institute for Research in Cystic Fibrosis, IERFC ONLUS Foundation, Ospedale San Raffaele, Via Olgettina, 58, 20132 Milano, Italy
[c]University of Piemonte Orientale, Department of Health Sciences, 28100 Novara, Italy

Abstract. Light sheet fluorescence microscopy has proven to be a powerful tool to image fixed and chemically cleared samples, providing in depth and high resolution reconstructions of intact mouse organs. We applied light sheet microscopy to image the mouse intestine. We found that large portions of the sample can be readily visualized, assessing the organ status and highlighting the presence of regions with impaired morphology. Yet, three-dimensional (3-D) sectioning of the intestine leads to a large dataset that produces unnecessary storage and processing overload. We developed a routine that extracts the relevant information from a large image stack and provides quantitative analysis of the intestine morphology. This result was achieved by a three step procedure consisting of: (1) virtually unfold the 3-D reconstruction of the intestine; (2) observe it layer-by-layer; and (3) identify distinct villi and statistically analyze multiple samples belonging to different intestinal regions. Even if the procedure has been developed for the murine intestine, most of the underlying concepts have a general applicability. [DOI: 10.1117/1.JBO.21.5.056001]

Keywords: three-dimensional microscopy; light sheet fluorescence microscopy; image processing.

Paper 150867R received Dec. 28, 2015; accepted for publication Apr. 1, 2016; published online May 2, 2016.

1 Introduction

Imaging methods like computer tomography,[1] magnetic resonance imaging,[2] photoacoustic tomography,[3] and fluorescence molecular tomography[4] offer the chance to three-dimensionally (3-D) image the full body of small animals, providing a breakthrough in experimental medicine. However, the analysis of some tissues, such as the intestine, is still problematic and can hardly be performed *in-vivo*, mainly due to organ length and spatial organization. Indeed, lesions induced in the intestine by disease models are often not homogeneously distributed along the entire gut length and even in control animals scattered lesions might be present, possibly due to either bacterial colonization, feeding procedures, or surgical stress during excision. Such lesions could account for both functional and histological variability even within intestinal regions with apparently normal morphology.[5,6] This entails the need of tissue examination endowed with cellular resolution together with the capability of analyzing in detail large tissue volumes. Currently, histology and immunohistochemistry/immunofluorescence analysis are widely applied to biological research, although the analysis of few tissue sections is not always representative of the entire intestinal architecture,[3,4,7] which can be highly variable along its extension. On the other hand, 3-D reconstruction from serial slices is not feasible for such a long organ.

In order to routinely analyze large portions of the intestine, we applied light sheet fluorescence microscopy (LSFM),[7–9] which has been demonstrated to be a powerful tool to image entire millimeter-scaled biological specimens, in depth and at high resolution. Combined with chemical clearing,[10] LSFM can image intact mouse organs, including brain,[11] spinal cord,[12] solid tumors,[13] lung, pancreas, and mammary glands.[14] Here, we show the results of LSFM applied to large portions of fixed and chemically cleared mouse intestines and we describe an automatic routine developed to quantify the villi density and to study the intestine morphology. Remarkably, by looking at the tissue autofluorescence, without any staining, we could visualize the 3-D shape of hundreds of villi in a single LSFM acquisition, taking advantage of the large field of view (ca. 3×3 mm^2) of the system. Yet, quantitative analysis was complicated by the large amount of data generated in each experiment and by the fact that image processing, segmentation, and quantification procedures had to be applied to the entire 3-D volume. We, therefore, decided to develop an imaging routine (hereby called "virtual unfolding"), which allows us to observe the intestine layer-by-layer, by applying a geometrical transformation that takes into account the shape of the organ. Successive segmentation of two-dimensional (2-D) layer images of the unfolded intestine permits villi count, clustering, and quantitative assessment of the anatomical features of the tissue. Here, we aim at validating the capability of this method to discriminate between intestinal regions exhibiting normal or impaired mucosal architecture.

2 Materials and Methods

2.1 *Optical Setup*

Fluorescence imaging was performed using a light sheet microscope (Fig. 1), whose optical system is substantially similar to the

*Address all correspondence to: Andrea Bassi, E-mail: andreabassi@polimi.it

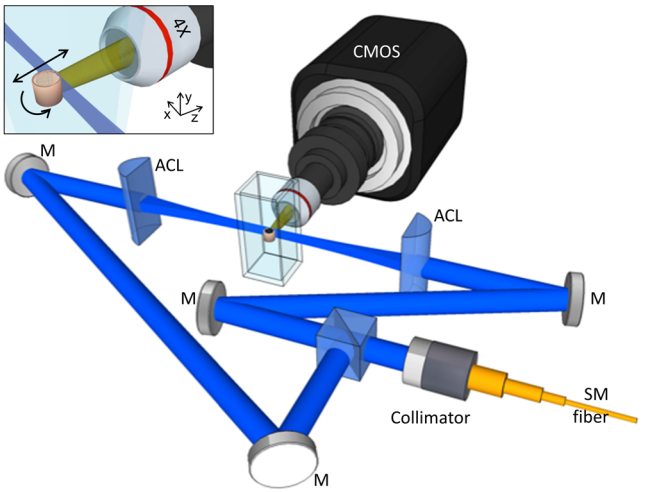

Fig. 1 Sketch of the optical setup. The sample is immersed in a glass cuvette filled with clearing liquid and is scanned though the detection image plane by a motorized stage (not shown). The displayed elements include the single-mode (SM) optical fiber, mirrors (M), achromatic cylindrical lens (ACL) and the CMOS camera.

ultramicroscope developed by Dodt.[11] To excite the autofluorescence, a diode-pumped solid-state laser emitting at 473 nm (CNI, MBL-FN-473) is coupled into a single-mode optical fiber that delivers the light to the setup. The laser beam is split into two portions in order to illuminate the sample from opposite sides: two cylindrical lenses ($f = 75$ mm) are used to create a light sheet made by two beams counter-propagating across the sample. The illumination power was 5 mW for each side. A chopper wheel in the illumination path allows one to illuminate the sample alternatively from opposing directions in order to reduce the effect of light sheet spreading caused by light scattering.[15] Rotation of the sample around 360 deg is also possible to support the multiview approach.[16] A 4× objective (Nikon, PLAN FLUOR, NA = 0.13) with a long working distance (17.2 mm) is used to collect the fluorescence emitted orthogonally to the light sheet. The objective, in combination with a tube lens (Nikon) and a long pass filter (FELH500, Thorlabs), forms the image of the fluorescence emission on a 4 MP CMOS camera (ORCA Flash 4.0, Hamamatsu, $n_x = 2048$ and $n_y = 2048$), with a field of view of ca. 3×3 mm^2. The lateral resolution was limited by the NA = 0.13 objective to about 2.3 μm and the later resolution was limited by the waist of the light sheet, which was 15 μm. The camera is synchronized with the chopper in order to alternatively acquire the fluorescence images corresponding to the two counter-propagating light sheets. Each pair of acquired images, corresponding to illumination from the two opposite sides, was computationally fused to yield superior image quality.[15] In particular, the halves of the images that present more artifacts (which are due to absorption and scattering of the excitation beams) were removed and the remaining two halves were merged using a stitching algorithm.[17] Exposure times were 100 ms for each plane, depending on the fluorescence signal. The typical number of acquired planes was $n_z = 400$, with steps of 10 μm and the total acquisition time was 40 s.

2.2 *Animals*

Six, 8-week-old, Balb C mice were prepared for the experiment using enforced gavage with water solution for three consecutive days. Then the mice were euthanized with an overdose of Avertine (tribromoethanol, 250 mg/kg; Sigma Aldrich, T48402) and the whole intestine was collected from each animal for analysis. All the procedures with mice were approved by the local Ethics Committee for Animal Welfare (IACUC N° 583) and were carried out in strict respect for European and National regulations.

2.3 *Sample Preparation and Measurement Procedure*

After excision, the intestines underwent fixation with formalin (Sigma Aldrich, F8775) at 4°C for 24 h, dehydration in methanol (33%, 66%, 100%, 15 min/step), overnight bleaching with freshly prepared MeOH:H_2O_2:DMSO buffer in a 2:1:3 ratio, and chemical clearing in a 1:2 solution of benzyl alcohol-benzyl benzoate (BABB) to reduce optical scattering. The samples were then cut into chunks approximately 10 mm long. For the LSFM experiment, each piece was held in place in a cuvette filled with BABB using small tweezers and moved through the light sheet, using a motorized translation stage (PI, M-405.CG) to obtain a 3-D image stack.

2.4 *Virtual Unfolding*

The application of LSFM to each intestine sample led to an image stack of about $3 \times 3 \times 3$ mm^3 volumes with $n_x \cdot n_y \cdot n_z$ voxels. The dataset can be visualized in Cartesian coordinates along transverse, sagittal, and coronal sections (Figs. 2 and 3) or in 3-D reconstructions. Nevertheless, such views do not match the geometry of the sample, which could be better analyzed in a reference system based on the external shape. More specifically, the sample could be conveniently visualized layer by layer, from the outward surface to the inner bore, or vice versa. For this purpose, we processed the acquired dataset using an automatic routine that projects the sample in an appropriate framework (Fig. 4). The procedure consists of

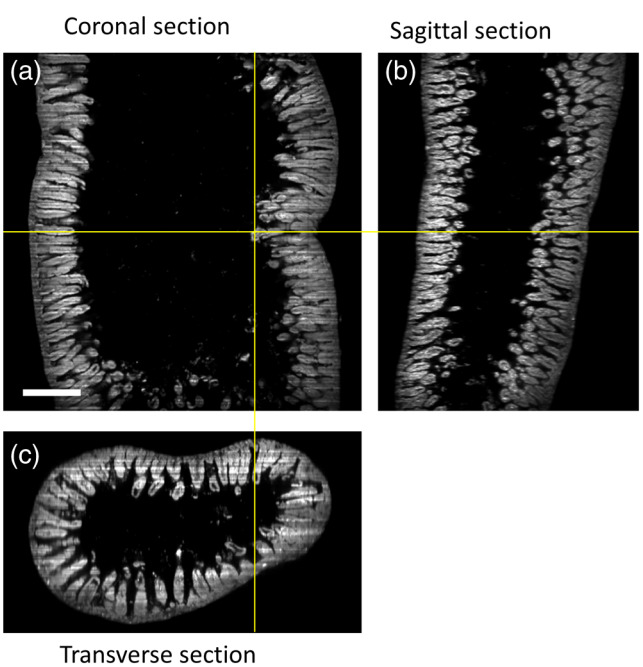

Fig. 2 Sections of the sample. (a) Coronal section, (b) sagittal section, and (c) transverse section. Scale bar 500 μm (Video 1, 6.98 MB) [URL: http://dx.doi.org/10.1117/1.JBO.21.5.056001.1]..

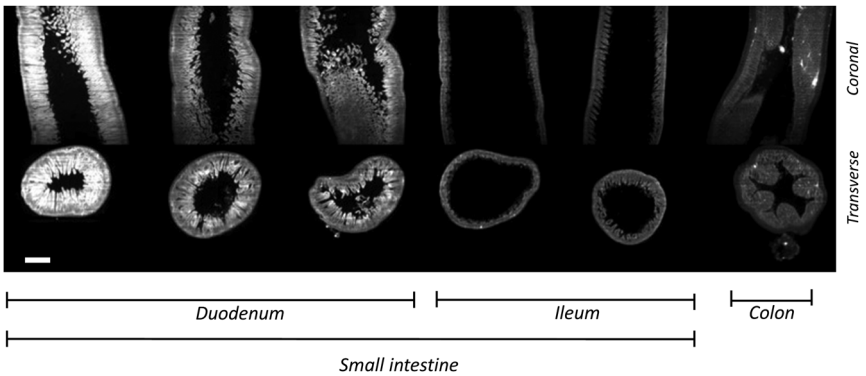

Fig. 3 Coronal and transverse sections of an untreated intestine in different anatomical regions. Scale bar 500 μm.

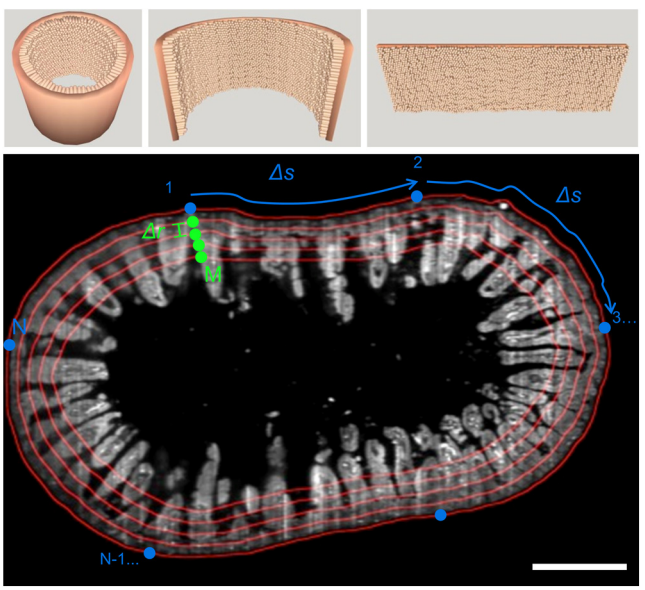

Fig. 4 Upper panels: scheme of the procedure: a sample with cylinder-like shape is "unfolded" and projected to a planar geometry. Lower panel: scheme of the procedure that allows one to select *N* points that lay on each of the *M* layers of the tissue. The procedure is repeated in all the transverse sections of the sample. Scale bar 500 μm.

1. segmentation and smoothing of the entire intestine volume in order to provide the boundaries of the organ;
2. extraction of the i'th transverse section, which shows a pseudoannular geometry, as a consequence of the elongated shape of the tissue;
3. sampling of N points along the external perimeter of the segmented intestine in the i'th transverse section; these points are at a distance Δs, which corresponds to the perimeter of the section divided by N;
4. morphological erosion over a distance Δr performed on the segmented intestine in the i'th transverse section;
5. sampling of a new set of N points along the new perimeter of the intestine resulting from the erosion;
6. repetition of steps (4) and (5) for a number of times M required to reach the inner bore of the segmented intestine in the i'th section; and
7. repetition of the procedure steps (2) to (6) all over the n_y transverse sections.

The method creates $M \times N$ new point-like samples in each of the n_y transverse sections, leading to a new image stack of $M \times N \times n_y$ voxels that contains only the relevant information, because the majority of the meaningless voxels (black voxels) inside and outside the intestine are removed. This usually brings a reduction of about twofold of the dataset. More importantly, this new dataset results from the projection of the original one onto a reference system based on the shape of the sample, which is more suitable for the analysis of the tissue morphology. In particular, the 2-D images of M tissue layers, spaced one another by a quantity Δr, are intrinsically embedded in the dataset and can be easily displayed and processed.

The processing is run automatically once the user selects a threshold for segmentation, the sampling distance Δs_0, and the total distance $M \cdot \Delta r$. The distance Δs_0 indicates the spatial sampling on the surface of the sample. The distance $M \cdot \Delta r$, that determines the inner position in which the processing is stopped was normally 300 μm for the analyzed intestines (with $M = 100$). The value N was determined by the sampling distance Δs_0, which normally is equal to or is a multiple of the pixel size. Depending on the sample size, N was between 3000 and 6000. Since the perimeter of the sample decreases during the erosion, Δs decreases as well. This means that different layers are characterized by different sizes. For this reason, each layer is stretched (with a linear interpolation) by a factor $\Delta s/\Delta s_0$, creating a stack of layers that are aligned.

The data processing required ca. 4 min per stack with a i7 4930 CPU, 3.4 GHz. The MATLAB code for virtual unfolding is available upon request.

2.5 *Segmentation of the Villi*

Villi segmentation was performed on the M images of the intestine layers obtained after the virtual unfolding procedure. The so called "watershed segmentation" method,[18] consisting of a series of grayscale morphological image processing operations was implemented in MATLAB. Each villus was automatically colored to distinguish it from adjacent ones. The code for segmentation is available upon request.

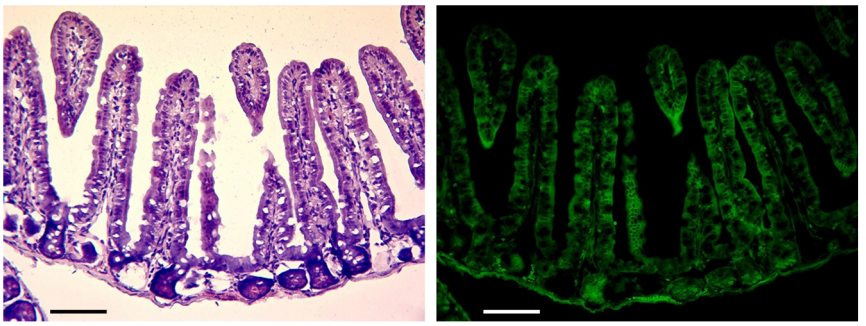

Fig. 5 Thin section of a fixed intestine sample. (a) H&E and (b) autofluorescence. Scale bars 100 μm.

3 Results and Discussion

3.1 *Reconstruction of Large Portions of the Intestine with Light Sheet Fluorescence Microscopy*

We observed strong and similar autofluorescence intensities in the mucosa and muscular tissues of different intestine samples. Biological tissues exhibit a noticeable autofluorescence that can be ascribed to several fluorophores. Among them, we can mention amino acids, structural proteins, notably collagen and elastin, the coenzyme nicotinamide adenine dinucleotide in the reduced form (NADH), and flavin derivatives, like riboflavin.[19,20] An increase in tissue autofluorescence is also rather common after fixation with formalin due to cross-link of dopamine.[21,22] In the specific case of the intestine, considering the excitation (473 nm) and the emission (>500 nm) wavelengths, the most likely candidates for the autofluorescence observed in the present experiment are flavin derivatives, like the flavin mono (FMN) and dinucleotide (FAD), with possible contributions from lipopigments, like lipofuscin, and enteramine.[23] All these fluorescent compounds have been documented to contribute to the intestine autofluorescence upon excitation with two photons, roughly corresponding to blue light.[24] As a matter of fact, the fluorescence observed in a thin section of fixed intestine is strong, as shown in Fig. 5. In order to assess the morphology of the intestine in various regions, we imaged the tissue autofluorescence and visualized the acquired volumes in different planes (sections) or in 3-D renderings (Fig. 2 and Video 1).

LSFM provided high-resolution volumetric reconstruction of the samples, showing fine anatomical details of villi, glands, and muscular tissue. In particular, the muscular tissue close to the outer surface of the sample was clearly recognizable by the typical circularly shaped muscular cells aggregates (Video 1). Remarkably, light-sheet shadowing effects caused by light attenuation, which occasionally downgrade the image quality in LSFM, were very limited over the entire intestine. This is likely due to the low density of the intestinal tissue compared to, e.g., brain or spinal cord. Moreover, the sample presents a cavity in its center, which contributes to reduce the attenuation of the excitation light. Indeed, the multiview acquisition was not necessary and high quality reconstructions of 2- to 3-mm-thick intestine tissues were obtained in a single scan. The high quality achievable with a single acquisition facilitates the analysis of a large number of samples, reducing the time required for alignment and image acquisition. Multiple view acquisition could be used to further improve the resolution or to achieve isotropic resolution, but at the cost of longer acquisition and processing time, which is not always compatible with the fact that one may need to analyze hundreds of samples in a clinical study.

Various regions of the intestine, representative of different anatomical districts (duodenum, ileum, colon), are shown in Fig. 3. We observe that the autofluorescence intensity decreases going from the upper tract of the intestine (duodenum) to the

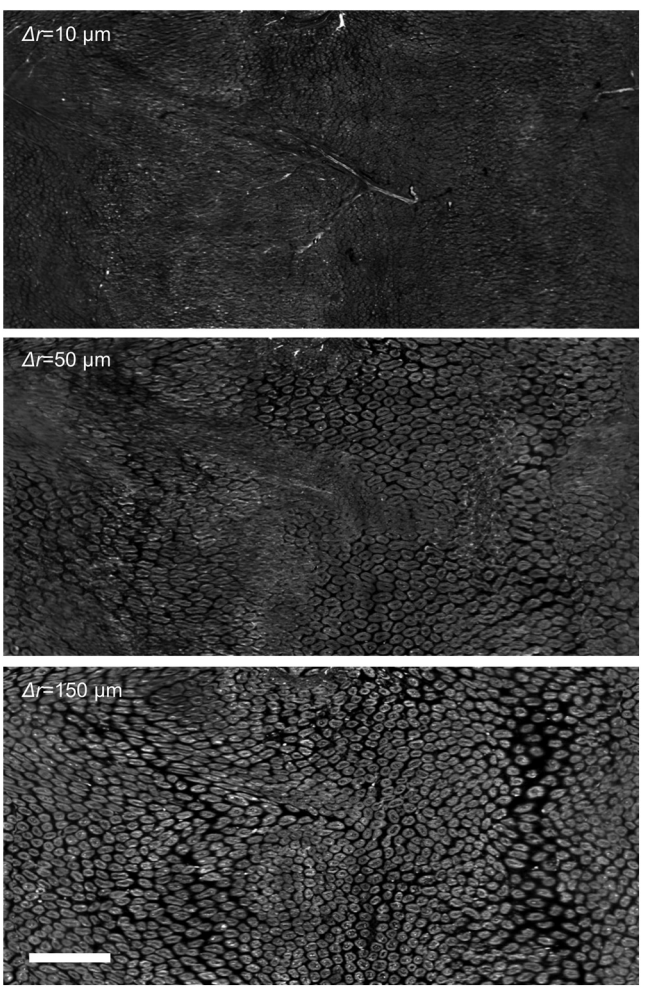

Fig. 6 Results of the unfolding procedure. Layers of the intestine are visualized at three different locations (depths) showing vessels and muscular structures as well as the mucosa with its villi. Scale bar 500 μm.

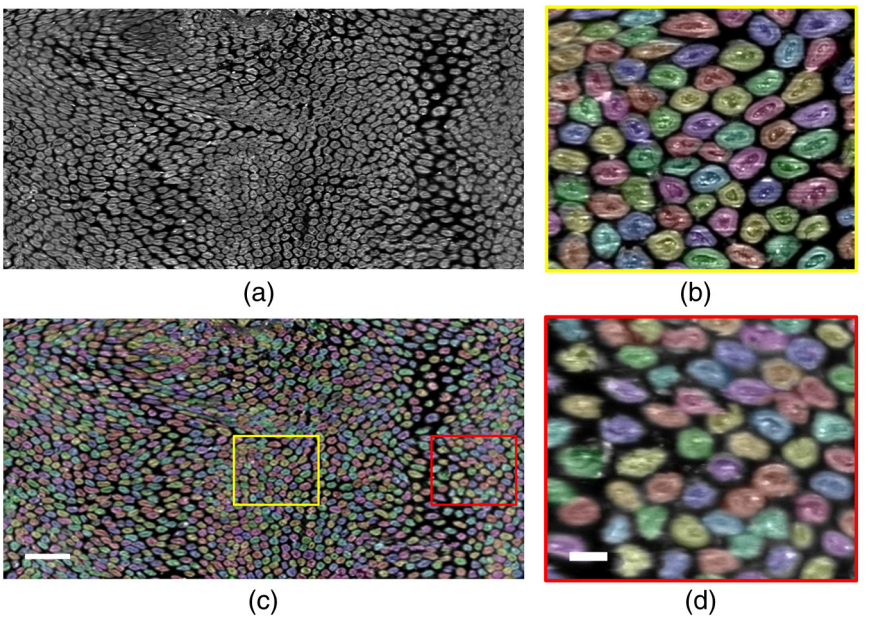

Fig. 7 Results of the segmentation analysis. (a) Original layer obtained after unfolding at a depth of ca. 150 μm inside the tissue. (c) Segmented image. (b and d) details of the segmentation in two regions, corresponding to the dorsal and frontal part of the tissue. Scale bars 500 μm (left) and 100 μm (right).

lower part (colon). This decrease was systematically observed in all the samples that were entirely analyzed ($n = 6$). Conversely, the distribution and shape of the villi, the morphology of the wall, and of the internal structure of the organ are clearly distinctive along the different tracts.

3.2 *Layer by Layer Visualization*

A detailed analysis of villus morphology, coupled to a quantitative spatial assessment of villi density along the intestine, is mandatory to either detect or monitor the extension of the putative intestinal lesions along its whole length.[8] Although a large number of distinct villi could be imaged at high resolution in each acquired region, quantification of their density was computationally expensive and inaccurate within the 3-D volume. Using the standard imaging approach, a relatively large amount of data (>4 GB) was accumulated for each acquisition, leading to a strong computational effort for the segmentation of the different compartments and the localization of the villi. In particular, identification of villi was challenged by the fact that they could lay in any direction within the 3-D volume. Moreover, the majority of the stored data corresponded to black pixels belonging to the volume external to the tissue and to its internal cavity. We, therefore, looked for a more efficient way to visualize and process the image stacks.

For this purpose, we developed an algorithm to virtually unfold the intestine around its external surface by exploiting its cylinder-like shape. The algorithm projects the layers of the sample in a planar geometry (Fig. 4, upper panels). A similar method was proposed by Schmid et al.[25] for spherically shaped specimens. Yet, although the intestine presents a cylindrical symmetry in many tracts, this is not the case along its whole length. Hence, a simple extension of the Schmid method to the projection of the dataset into a cylindrical coordinate system could not be applied. As an alternative method, we tried to sample the inner layers of the tissue by selecting a sequence of equally spaced points along the set of lines normal to the boundary of the sample. Yet, this method was too sensitive to the unevenness of the outer surface of the intestine that led to unacceptable segmentation noise. This problem has been recently solved by generating a smooth model of the surface of interest by fitting the segmented volume or through triangulation.[26]

Alternatively, we devised a virtual unfolding routine based on morphological operations that takes into account the shape of the intestine. Each layer was obtained by the erosion of the external boundary of the organ, as described in Sec. 2. This approach can be applied in principle to any geometry, because the layers can be obtained by applying the morphological erosion directly to the 3-D model. However, in order to process the dataset more rapidly, we applied the method to each transverse section of the acquired stack, taking advantage of the elongated shape of the intestine.

3.3 *Quantification of Villi Density, Shape and Morphology*

Once the intestine was virtually unfolded, we could navigate through its volume, layer by layer (Fig. 6). Going inward from the outer boundary, the first layers of the intestine are characterized by the presence of the superficial vessels and the muscular tissue. Going deeper, a transition region, rich in muscular tissue and villi, is observed. Finally, the villi that protrude from the epithelial lining of the intestinal wall are reached and cut perpendicularly to their axis (Fig. 6, lower panel). In each 2-D unfolded image, hundreds of villi are sectioned, producing a significant assay of their morphology, density, and shape. The sampling of each layer is performed at a constant distance Δs along the perimeter of the transverse sections of the specimen. This is crucial to reduce the deformations that would have been caused by projecting the sample to a simple cylindrical geometry. Indeed, the majority of the villi are cut transversally by the layers (Fig. 4), providing an accurate reconstruction of their shape in the new coordinate system. However, because

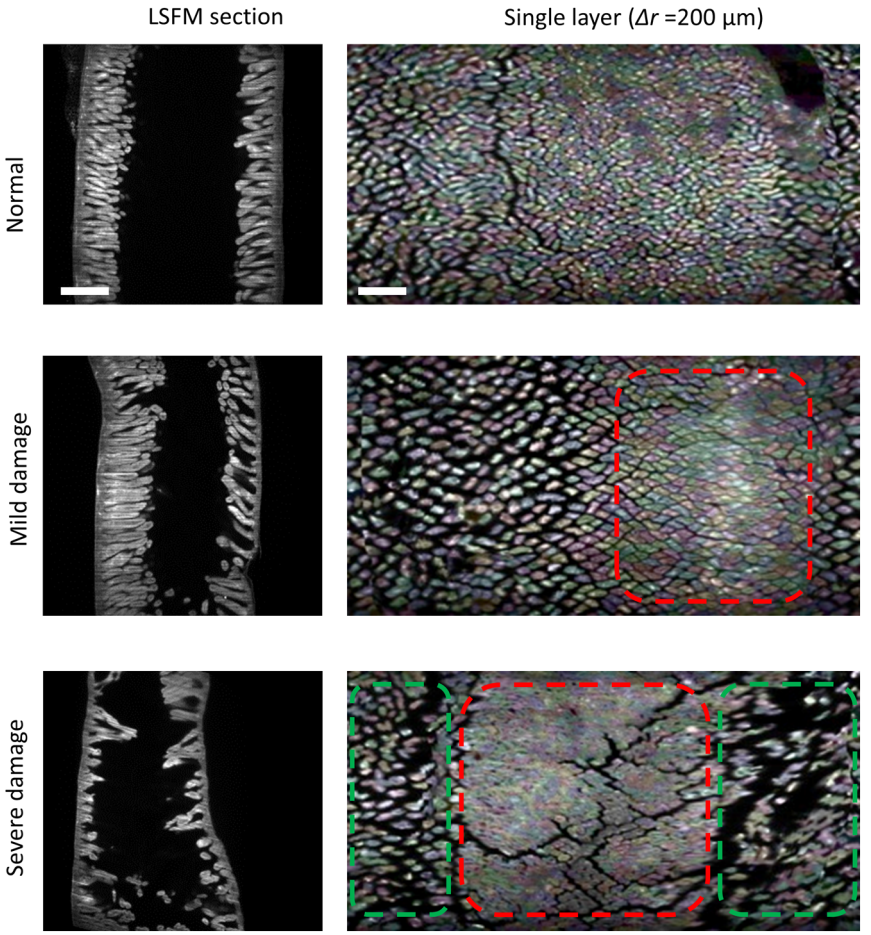

Fig. 8 Representative intestines showing no damage (normal), mildly and severely damaged tissues. At 200 μm in depth from the outer surface of the intestine, the unfolded layers (right side) show hyperplastic regions (red) and atrophic regions (green). Scale bars 500 μm.

of the irregular morphology of the tissue, some villi are cut obliquely or unevenly by the layer, particularly in the highly curved region of the sample. This can cause deformation of their shape (e.g., they can appear elliptical), but overall their number and density can still be measured accurately. The quantification of the villi number and density was accomplished in the new coordinate system using standard watershed segmentation (see Sec. 2). In Fig. 7, each segmented villus is shown in a different color. The separation between adjacent villi and the sharpness of the image indicates that not only the density and distribution of the villi can be obtained, but also their position and shape can be statistically analyzed. Looking at more details in the image of a layer and at the segmentation of the villi (colored panels in Fig. 7), we observe that the image quality varies along the horizontal direction. In fact, because of the unfolding, the center of the image corresponds to the portion of the sample closer to the microscope objective, while the extremities correspond to the back side. Hence, it is not surprising that the center of the image shows a resolution higher than the left and right borders: this difference is due to the scattering of the fluorescence emission while propagating through the sample toward the objective. Here, multiview acquisition would have improved the image quality of the dorsal region. However, the resolution obtained with a fast single-view scan was sufficient for accurate segmentation of the villi in the entire image.

It is worth noting that Fig. 7 shows the result of an automatic segmentation. Comparison with manual segmentation of the villi showed a difference lower than 5% across the entire image. Hence, taking advantage of the quality of the images achieved with the unfolding procedure and of the layer navigation method, we were able to segment and statistically compare the anatomical features of multiple samples.

In two out of six mice, we see clear differences in shape and density of villi (Fig. 8, left side), mainly in the duodenum tract of the intestine. In this region, the normal villi density is $\delta = 76 \pm 15$ mm^{-2} ($n = 6$), calculated as the number of segmented villi divided by the outer surface of the 3-D volume. Such a lesion is variable among mice as well as along the whole intestine. Some mice developed a segmental hyperplastic lesion, with conserved density of villi, but enlarged villous size (region inside the red rectangle in the central panel of Fig. 8), others showed severe lesions creating regions characterized by flattened villi and crypt hyperplasia with reduction in villi density with respect to the outer surface (region inside the green rectangle in the lower panel of Fig. 8).

These results indicate that the analysis of intestine lesions is feasible in terms of the density of villi, which can be measured with an automatic procedure. The proposed method, based on LSFM, has several advantages with respect to serial histological sectioning. Most of all, large portions of the intestine can be analyzed in a quantitative way with minimal preparation of

the sample, no staining or labeling, and fast acquisition and processing of data.

Many intestinal diseases, such as coeliac disease or chronic inflammatory diseases, manifest a scattered lesion pattern that affects only parts of the entire organ, while others are preserved. In addition, intestinal lesions may be restricted to the mucosal surface or may also involve the whole mucosa within a selected region. The assessment of both severity and extension of intestinal lesions in experimental models of intestinal diseases, along with the putative improvement in mucosal architecture during treatment, must imply an accurate comparison with a reference "normal" counterpart. Thus, coupling wide-field and high-resolution imaging may represent a priceless tool to understand disease evolution as well to monitor the putative effects of treatments in animal models of disease.

4 Conclusion

In conclusion, we devised a new method based on LSFM to study the mouse intestine and to evidence the occurrence of segmental lesions in an animal model. The anatomical features of murine intestines could be clearly visualized by acquiring the autofluorescence signal emitted by the tissue. An automatic data processing routine allowed virtual unfolding of the intestine, based on its specific shape. Using this approach, rather than analyzing the sample in a complex 3-D geometry, we could image the intestine layer by layer, facilitating the segmentation of the anatomical structures and the assessment of the lesions. The morphology of anatomical features, like the external vasculature, the muscular layer, and the mucosa, could be visualized over large portions of the organ. This opens the way for a simple and effective approach to study established disease-related models of intestinal lesions as well as to monitor the effect of drug treatments in preclinical studies.

Finally, it is worth mentioning that the concepts underlying the proposed method, and in particular, the unfolding algorithm based on erosion operations have a general applicability and can be used to navigate inside any 3-D reconstruction of a whole mount specimen acquired with LSFM or other tomographic imaging methods, such as optical projection tomography.[27–29] This provides a new tool with potential wide application in experimental medicine.

Acknowledgments

The research leading to these results has received funding from LaserLab-Europe (EU-H2020 654148).

References

1. W. A. Kalender, "CT: the unexpected evolution of an imaging modality," *Eur. Radiol.* **15**, D21–D24 (2005).
2. J. M. Tyszka, S. E. Fraser, and R. E. Jacobs, "Magnetic resonance microscopy: recent advances and applications," *Curr. Opin. Biotechnol.* **16**, 93–99 (2005).
3. D. Razansky et al., "Deep tissue optical and optoacoustic molecular imaging technologies for pre-clinical research and drug discovery," *Curr. Pharm. Biotechnol.* **13**, 504–522 (2012).
4. G. Zacharakis et al., "In vivo whole-body molecular tomography of fluorescent proteins in small animals," *Proc. Natl. Acad. Sci. U.S.A.* **102**, 18252–18257 (2005).
5. R. Bowcutt et al., "Heterogeneity across the murine small and large intestine," *World J. Gastroenterol.* **20**(41), 15216–32 (2014).
6. L. A. Reynolds, B. B. Finlay, and R. M. Maizels, "Cohabitation in the intestine: interactions among helminth parasites, bacterial microbiota, and host immunity," *J. Immunol.* **195**(9), 4059–4066 (2015).
7. J. Huisken et al., "Optical sectioning deep inside live embryos by selective plane illumination microscopy," *Science* **305**, 1007–1009 (2004).
8. P. A. Santi, "Light sheet fluorescence microscopy: a review," *J. Histochem. Cytochem.* **59**(2), 129–138 (2011).
9. P. J. Keller and H. U. Dodt, "Light sheet microscopy of living or cleared specimens," *Curr. Opin. Neurobiol.* **22**(1), 138–143 (2012).
10. W. Spalteholz, *Über das Durchsichtigmachen von menschlichen und tierischen Präparaten*, S. Hirzel, Leipzig, Germany (1911).
11. H. U. Dodt et al., "Ultramicroscopy: three-dimensional visualization of neuronal networks in the whole mouse brain," *Nat. Methods* **4**(4), 331–336 (2007).
12. A. Ertürk et al., "Three-dimensional imaging of the unsectioned adult spinal cord to assess axon regeneration and glial responses after injury," *Nat. Med.* **18**(1), 166–171 (2011).
13. M. Dobosz et al., "Multispectral fluorescence ultramicroscopy: three-dimensional visualization and automatic quantification of tumor morphology, drug penetration, and antiangiogenic treatment response," *Neoplasia* **16**(1), 1–W7 (2014).
14. A. Erturk and F. Bradke, "High-resolution imaging of entire organs by 3-dimensional imaging of solvent cleared organs (3DISCO)," *Exp. Neurol.* **242**, 57–64 (2013).
15. J. Huisken and D. Y. R. Stainier, "Even fluorescence excitation by multidirectional selective plane illumination microscopy (mSPIM)," *Opt. Lett.* **32**, 2608–2610 (2007).
16. J. Swoger et al., "Multi-view image fusion improves resolution in three-dimensional microscopy," *Opt. Express* **15**, 8029–8042 (2007).
17. S. Preibisch, S. Saalfeld, and P. Tomancak, "Globally optimal stitching of tiled 3D microscopic image acquisitions," *Bioinformatics* **25**(11), 1463–1465 (2009).
18. L. Najman and H. Talbot, *Mathematical Morphology: From Theory to Applications*, John Wiley & Sons, Inc., Hoboken, New Jersey (2010).
19. S. Andersson-Engels et al., "In vivo fluorescence imaging for tissue diagnostics," *Phys. Med. Biol.* **42**(5), 815–824 (1997).
20. R. C. Benson et al., "Cellular autofluorescence - is it due to flavins?," *J. Histochem. Cytochem.* **27**(1), 44–48 (1979).
21. B. Falck et al., "Fluorescence of catechol amines and related compounds condensed with formaldehyde," *J. Histochem. Cytochem.* **10**(3) 348–354 (1962).
22. U. Leischner et al., "Formalin-induced fluorescence reveals cell shape and morphology in biological tissue samples," *PloS One* **5**(4), e10391 (2010).
23. R. Orzekowsky-Schroeder et al., "In vivo spectral imaging of different cell types in the small intestine by two-photon excited autofluorescence," *J. Biomed. Opt.* **16**(11), 116025 (2011).
24. W. Feldberg and C. C. Toh, "Distribution of 5-hydroxytryptamine (serotonin, enteramine) in the wall of the digestive tract," *J. Physiol.* **119**(2–3), 352–362 (1953).
25. B. Schmid et al., "High-speed panoramic light-sheet microscopy reveals global endodermal cell dynamics," *Nat. Commun.* **4**, 2207 (2013).
26. I. Heemskerk and S. J. Streichan, "Tissue cartography: compressing bio-image data by dimensional reduction," *Nat. Methods* **12**, 1139–1142 (2015).
27. J. Sharpe et al., "Optical projection tomography as a tool for 3D microscopy and gene expression studies," *Science* **296**, 541–545 (2002).
28. A. Arranz et al., "Helical optical projection tomography," *Opt. Express* **21**, 25912–25925 (2013).
29. A. Bassi, B. Schmid, and J. Huisken, "Optical tomography complements light sheet microscopy for in toto imaging of zebrafish development," *Development* **142**(5), 1016–1020 (2015).

Alessia Candeo is a research assistant at Politecnico di Milano. She received her BS and MS degrees in engineering physics in 2010 and 2012, respectively, and her PhD in physics in March 2016 from Politecnico di Milano. Her current research interests include laser science, spectroscopy and microscopy for biomedical applications.

Ilenia Sana received her master's degree in industrial biotechnology from University of Milan-Bicocca, Italy, in 2013. Since 2014 she has been a research assistant at the European Institute for Research in Cystic Fibrosis, San Raffaele Hospital, Milan.

Eleonora Ferrari is a research assistant at the European Institute for Research in Cystic Fibrosis, San Raffaele Hospital, Milan. She

received her BS degree in biotechnology and her MS degree in biology in 2009 and 2012, respectively, from Università degli studi di Milano-Bicocca. Her current research interests include cellular biology and animal models.

Luigi Maiuri is professor of pediatrics, University of Novara, and director of the European Institute for Cystic Fibrosis Research, San Raffaele Hospital, Milan. From 2002 to 2007 he was appointed as honorary senior lecturer at the University College of London and from 2008 to 2011 as visiting professor at the University of Southampton. His research focuses on understanding disease mechanisms and discovering new therapies to control disease evolution, principally in celiac disease and cystic fibrosis.

Cosimo D'Andrea received the PhD in physics from Politecnico di Milano in 2001. He is currently an associate professor at Dept. of Physics of Politecnico di Milano. His research interests include time-resolved fluorescence spectroscopy/imaging for study of biological samples and development of *in vivo* optical molecular imaging techniques.

Gianluca Valentini has been a full professor of physics and photonics at Politecnico di Milano since January 2011. He started his scientific career as a laser scientist in 1989. Presently, he is mainly involved in research on advanced fluorescence imaging and spectroscopy for medicine and biology. He also leads a research group on spectroscopy and imaging for the conservation of cultural heritage.

Andrea Bassi received his PhD in physics at Politecnico di Milano in 2006. He conducted research at Beckman Laser Institute, University of California (Irvine) in 2005 as research specialist, at Politecnico di Milano from 2006 to 2013 as a researcher, at Max Planck Institute (Dresden) in 2013 as Marie Curie Fellow. Currently he is an associate professor of physics of Politecnico di Milano. His scientific interests include optical microscopy for biological and preclinical applications.